

Design of Selective, ATP-Competitive Inhibitors of Akt[†]

Kevin D. Freeman-Cook,* Christopher Autry, Gary Borzillo, Deborah Gordon, Elsa Barbacci-Tobin, Vincent Bernardo, David Briere, Tracey Clark, Matthew Corbett, John Jakubczak, Shefali Kakar, Elizabeth Knauth, Blaise Lippa, Michael J. Luzzio, Mahmoud Mansour, Gary Martinelli, Matthew Marx, Kendra Nelson, Jayvardhan Pandit, Francis Rajamohan, Shaughnessy Robinson, Chakrapani Subramanyam, Liuqing Wei, Martin Wythes, and Joel Morris

Pfizer Global Research and Development, Eastern Point Road, Groton, Connecticut 06340

Received March 26, 2010

This paper describes the design and synthesis of novel, ATP-competitive Akt inhibitors from an elaborated 3-aminopyrrolidine scaffold. Key findings include the discovery of an initial lead that was modestly selective and medicinal chemistry optimization of that lead to provide more selective analogues. Analysis of the data suggested that highly lipophilic analogues would likely suffer from poor overall properties. Central to the discussion is the concept of optimization of lipophilic efficiency and the ability to balance overall druglike properties with the careful control of lipophilicity in the lead series. Discovery of the nonracemic amide series and subsequent modification produced an advanced analogue that performed well in advanced preclinical assays, including xenograft tumor growth inhibition studies, and this analogue was nominated for clinical development.

Introduction

Akt (PKB)^a is a serine/threonine kinase that plays a central role in promoting cell survival. Akt denotes a family of kinases (Akt1, Akt2, Akt3) with tissue-specific patterns of expression that can include the coexpression of multiple family members in normal tissues and tumors.^{1–3} Akt is part of a pathway that encompasses multiple receptor tyrosine kinases (PI3K and mTOR) and integrates extracellular signals with cell growth, proliferation, and survival. Akt activity is often deregulated in malignant cells, and evidence continues to accumulate that Akt is a promising point of therapeutic intervention for many cancers.^{4,5} Akt is located at a critical junction of multiple oncogenic and tumor suppression signaling pathways. Deregulation of Akt through inactivation of PTEN,⁶ point mutation, or overexpression can result in aberrant signaling.⁷ High levels of Akt activity are observed in a large number of human cancers and are correlated with poor prognosis and resistance to chemotherapy.^{8,9}

Because it encompasses such promising targets for cancer treatment, the PI3K–mTOR pathway in general, and Akt specifically, has generated substantial interest in the scientific community.^{10,11} Within the pharmaceutical industry, multiple

therapeutic approaches have been reported,^{12–14} including the use of rapamycin and small molecule analogues as mTOR inhibitors,^{15–18} PI3K inhibitors,^{19,20} PI3K/mTOR dual inhibitors,^{21–23} and inhibitors that modulate Akt activity in both a direct ATP-competitive^{24–30} and an indirect (allosteric)^{31–38} fashion. Continued reports of tumor growth inhibition with Akt inhibitors in animal models reflect ongoing attempts to interfere with this pathway and in some cases to include Akt inhibitors in combination with other treatment strategies.^{26,39,40}

Results and Discussion

Our work started with high-throughput screening against the kinase domain of Akt1 in an effort to identify ATP-competitive inhibitors for further medicinal chemistry optimization. A description of this approach, which led to the discovery of **1** and its subsequent optimization to **2** (Figure 1), was recently published.³⁹

While spiroindoline **2** represented a substantial improvement in potency over the initial leads and an important investigational compound demonstrating tumor growth inhibition (TGI), it had several undesirable properties. These included a distinct lack of selectivity against many other kinases (particularly vs the

[†]The X-ray coordinates of compound **5** bound to Akt1 and PKA have been deposited in the Protein Data Bank with accession numbers 3MV5 and 3MVJ. The X-ray coordinates of compound **42** bound to Akt1 have been deposited in the Protein Data Bank with accession number 3MVH.

*To whom correspondence should be addressed. Phone: 858-526-4844. Fax: 860-686-5036. E-mail: kevin.freeman-cook@pfizer.com.

^aAbbreviations: ACN, acetonitrile; Akt, protein kinase B (encompassing Akt1, Akt2, and Akt3); BOC, *tert*-butyl carbamate; DCM, dichloromethane; DIPEA, diisopropylethylamine; DMF, dimethylformamide; DMSO, dimethyl sulfoxide; GSK-3, glycogen synthase kinase 3; hERG, human ether-a-go-go-related gene; HLM Er, human liver microsome extraction ratio; HOBt, 1-hydroxybenzotriazole; LAH, lithium aluminum hydride; LipE, lipophilic efficiency; MeOH, methanol; mTor, mammalian target of rapamycin; PI3K, phosphoinositide 3-kinases; PKA, protein kinase A; PKB, protein kinase B (Akt); PTEN, phosphatase and tensin homologue; TEA, triethylamine; TFA, trifluoroacetic acid.

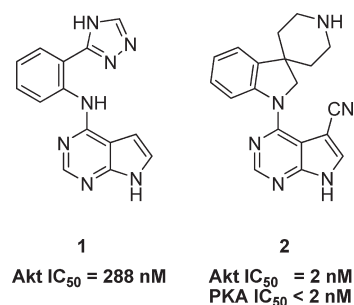
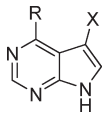
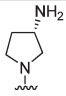
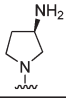
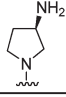
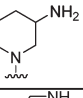
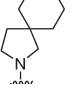


Figure 1. Aniline triazole **1** and spiroindoline **2**.

Table 1. New Scaffold Identification^a


Compound	R	X	Akt Kinase IC ₅₀ (nM)	PKA Kinase IC ₅₀ (nM)	PKA Selectivity Ratio
3		Cl	240	230	1.0
4		Cl	68	1300	19.1
5		CH ₃	180	3200	17.8
6		Cl	200	20	0.1
7		Cl	4	5	1.3

^aThe values are reported as the geometric mean of at least two separate determinations, with a typical standard variation of less than $\pm 30\%$. The PKA selectivity ratio is calculated using the following formula: PKA selectivity = (PKA IC₅₀)/(Akt IC₅₀).

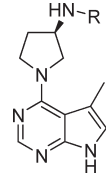
Table 2. Initial Kinase Selectivity Data^a

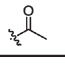
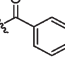
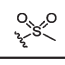
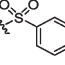
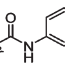
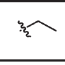
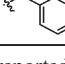
Kinase	Compound	
	2	5
Akt	100	98
PKA	99	ND
PKC	99	16
Abi	48	2
CHK1	49	17
CK2	8	< 2
c-kit	< 2	< 2
EGFR	38	< 2
Fit1	70	10
JNK2	8	< 2
MAPKAP-K2	43	< 2
MEK1	71	21

^a Values shown are % inhibition data at 1 M, and reflect the mean of at least two experiments.

highly homologous family member PKA) and a generally poor safety profile in animal studies. This compound exhibited dramatic effects on the GI tract and consequently had a very low projected therapeutic index (TI). An early hypothesis linked its low overall kinase selectivity with its low TI, supported by the finding that a structurally similar but kinase-inactive homologue of **2** had significantly diminished GI toxicity.⁴¹ Thus, an effort to discover new, more selective kinase inhibitors was initiated utilizing high speed parallel chemistry.³⁹

In this effort, potential new scaffolds were investigated by replacing the spiroindoline substituent of **2** by thousands of structurally diverse amines. The data for selected analogues are shown in Table 1. Most scaffolds were deliberately chosen to incorporate basic primary or secondary amines that could

Table 3. Amine substituent SAR expansion^a


Compound	R	Akt Kinase IC ₅₀ (uM)	PKA Kinase IC ₅₀ (uM)	PKA Selectivity Ratio
8		10	0.1	0.01
9		0.7	0.9	1.3
10		4	1.6	0.4
11		0.6	0.8	1.3
12		0.7	5.6	8.0
13		1.9	3.1	1.6
14		2.4	1.1	0.5

^aThe values are reported as the geometric mean of at least two separate determinations, with a typical standard variation of less than $\pm 30\%$.

be utilized for further elaboration. In general, even when potent starting points (e.g., **6** and **7**) were identified, they exhibited a disappointing level of selectivity for Akt over PKA. In contrast, the unique selectivity displayed by the 3-aminopyrrolidine series of analogues provided a compelling entry for further investigation.

The (3*R*)-aminopyrrolidine enantiomer **4** was both potent and 19-fold selective for Akt over PKA. The (3*S*)-enantiomer **3**, on the other hand, was somewhat less active (240 nM) and displayed equivalent activity against Akt and PKA. The fact that **5** displayed a similar level of selectivity to **4** suggested that the (3*R*)-aminopyrrolidine was responsible for conferring selectivity, regardless of small modifications at C-5 of the core pyrrolopyrimidine. Compounds **2** and **5** were subjected to further broad kinase profiling, which demonstrated an overall high level of selectivity for compound **5**, as shown in Table 2.

Our initial approach to elaboration of the (3*R*)-aminopyrrolidine scaffold involved derivatization of the basic amine. By use of standard parallel chemistry transformations, amides, sulfonamides, and ureas were prepared; the amine was also alkylated via reductive amination reactions.

Disappointingly, all of these compounds, a sample of which is shown in Table 3, lost potency against Akt. More significantly, they exhibited reduced or reversed selectivity versus PKA. The loss of potency alone may not have been impossible to overcome; however, the difficulty in achieving selectivity against this target in general argued that these modifications were disrupting an important interaction, and thus, it would be extremely challenging to reconstruct a reasonable level of selectivity. Ultimately, crystal structures of **5** in the kinase domains of both Akt and PKA (Figure 2a and 2b, respectively) provided a structural explanation for the observed loss of selectivity.

The X-ray structure of **5** in the active site of Akt (Figure 2a) revealed that the C-3 primary amine is displayed in a

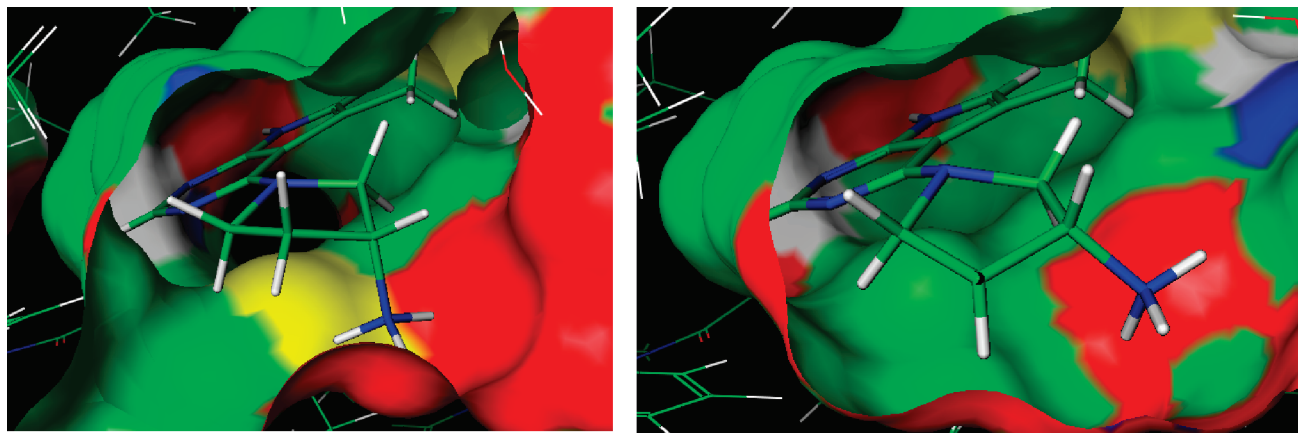
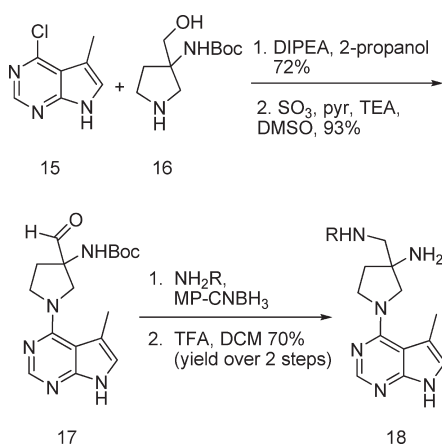


Figure 2. X-ray structures of **5**: (a, left) bound to Akt1; (b, right) bound to PKA.

Scheme 1. Synthesis of 3,3-Disubstituted Analogues



pseudoaxial orientation and forms a salt bridge to Glu-234, an interaction that would not be possible for the bulkier derivatized analogues. On the basis of this structural information, we proposed that introduction of substitution at the C-3 methine would lock the amine into the required pseudoaxial conformation while simultaneously providing an additional vector for optimization of binding potency.

Analysis of the crystal structure of PKA with **5** (Figure 2b) supported the hypothesis that this would be an effective strategy to maintain selectivity. Examination of the C-3 pyrrolidine methine proton in the PKA structure indicated that any extension at that position would likely result in a steric clash with nearby residues. Modeling the effect of adding even a single methyl group in place of the C-3 methine revealed a dramatic decrease in predicted binding affinity for PKA, while the corresponding binding in Akt was undisturbed. Together, these observations provided a compelling rationale to prepare the C-3 substituted pyrrolidine analogues.

The approach to derivatization at the 3-position utilized BOC-protected aminopyrrolidine **16** bearing a 3-hydroxymethyl group (Scheme 1).⁴² Addition to chloropyrrolopyrimidine **15** proceeded smoothly. After oxidation and reductive amination, the Boc was removed to reveal the elaborated aminopyrrolidine analogues **18**.

In the first set of compounds, anilines were installed during the reductive amination step (Table 4). Unsubstituted aniline **19** was found to be similarly potent and selective compared to the original aminopyrrolidine **5**, even when **19** was tested as a racemate. When **19** was separated into its two

Table 4. Initial SAR in the 3-Amino-3-Anilinomethylpyrrolidine Series

compd	R	chirality	Akt kinase IC ₅₀ (nM) ^a	PKA selectivity ratio	clogP	LipE	HLM Er ^b
19	—H	<i>rac</i>	160	15.7	2.3	4.5	0.64
19a	—H	<i>ent1</i>	3500	2.7	2.3	3.2	0.75
19b	—H	<i>ent2</i>	56	22.7	2.3	5.0	ND
20	—Me	<i>rac</i>	120	31.4	2.8	4.1	0.60
21	—Cl	<i>rac</i>	58	37.5	3.3	3.9	0.61
22	—CF ₃	<i>rac</i>	61	20	3.7	3.5	0.75
23	— ⁱ Pr	<i>rac</i>	50	50.9	3.7	3.6	0.73
24	—OPh	<i>rac</i>	16	51.2	4.4	3.4	0.73

^aThe values are reported as the geometric mean of at least two separate determinations, with a typical standard variation of less than $\pm 30\%$. ^bEr is the in vitro hepatic extraction ratio, which is obtained from dividing estimated hepatic blood clearance of test compounds by the human hepatic blood flow of 20 (mL/min)/kg. Protocols for measuring half-lives in HLM and further scaling to blood clearance have been published (see ref 44).

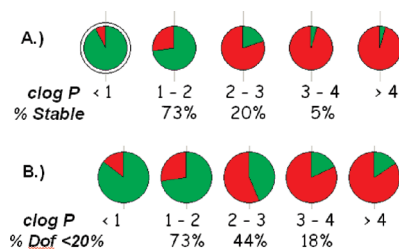
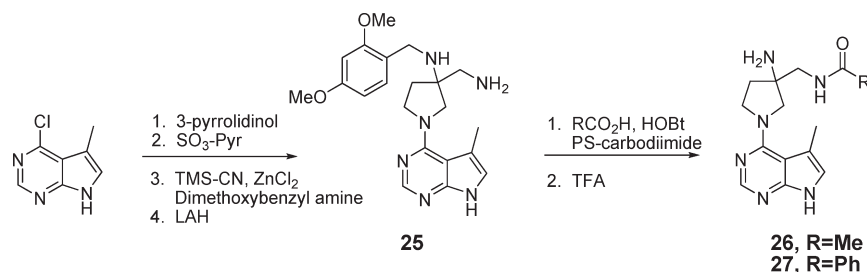
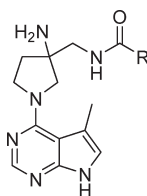


Figure 3. Pie charts showing the probability of success in higher log *P* space: (A) HLM stability. Stable compounds (HLM Er < 0.5) are represented in green, and the overall percentages of stable compounds are shown below the respective pie charts. (B) Dofetilide activity. Low dofetilide activity compounds (Dof, < 20% at 3 μ M) are represented in green, and the overall percentages of compounds with low dofetilide activity are shown below their respective pie charts.

enantiomers (**19a** and **19b**), one was both more potent and more selective while the other was substantially poorer in both respects.⁴³

Since the enantiomerically pure substituted 3-aminopyrrolidine confirmed our structural design hypothesis, we undertook

Scheme 2. Modified Synthesis for Preparation of Racemic Amides**Table 5.** SAR of Racemic Amide Analogues^a

compd	R	substituent	substituent position	Akt kinase IC ₅₀ (nM)	clogP	LipE	HLM Er
26	Me	none		765	0	6.1	ND
27	Ph	none		62	1.7	5.5	ND
28	Ph	-F	ortho	44	1.6	5.7	0.39
29	Ph	-F	meta	38	2	5.4	0.39
30	Ph	-F	para	7.4	2	6.1	0.46

^aThe values are reported as the geometric mean of at least two separate determinations, with a typical standard variation of less than $\pm 30\%$.

the synthesis of additional analogues (Table 4). To illustrate a trend, only a subset of ortho-substituents is shown. These modifications consistently showed improved potency as a result of increased lipophilicity. Unfortunately, the Akt potency gain was offset by a corresponding loss in human microsomal stability relative to **3**, a low clearance compound with HLM Er < 0.30.⁴⁴ Further examination of the data revealed that this was generally true in this series and not specifically related to the SAR of the ortho-position of the aniline. Lipophilic substituents generally provided potency enhancements. However, the net effects of increased clearance and increased hERG binding^{45–47} made these lipophilic analogues unattractive for further study. An analysis of the trends for in vitro clearance (Figure 3A) and dofetilide binding (Figure 3B), made evident by binning the data, revealed that subsequent designs would likely need to be targeted at clogP < 3. At clogP > 3 there was little chance of achieving both low clearance and low hERG binding.

At this point, the focus changed from identifying the most potent compounds to identifying those compounds with the most activity per unit of lipophilicity (the highest LipE).^{48,49} Theoretically, these would provide the best starting points for optimization with respect to the log *P* parameters outlined above and directly address multiple liabilities of this series. Additionally, consideration of LipE allows the identification of truly beneficial SAR as opposed to potency gains that are simply the consequence of large lipophilicity increases.

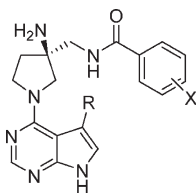
Modification of the synthetic route (Scheme 2) gave access to the valuable amine intermediate **25** in racemic form. Addition of 3-pyrrolidinol to 4-chloro-5-methyl-7H-pyrrolopyrimidine proceeded smoothly in the presence of Hunig's base. Oxidation of the resulting alcohol to the corresponding ketone with SO₃-pyridine complex was followed by a modified Strecker reaction with dimethoxybenzylamine using TMS-CN and ZnCl₂ as a Lewis acid.⁵⁰ Reduction of the nitrile with lithium aluminum

hydride produced the valuable amine intermediate **25**, which could be manipulated in a variety of standard transformations. To reduce the lipophilicity of the series, amide analogues were prepared by coupling of carboxylic acids followed by TFA-mediated cleavage of the dimethoxybenzyl protecting group.

Acetamide **26**, prepared in racemic form (Table 5), emerged as a notable analogue from this effort. This compound, while 300-fold weaker than derivatives that were being prepared in parallel in the aniline series, was a significant step forward in terms of LipE (6.1 vs 4.5 for aniline **19**). In contrast to compound **19**, the high LipE of **26** coupled with its clogP of 0 suggested that the judicious addition of lipophilicity within the amide framework could drive an increase in potency while still remaining within the defined high probability space (clogP < 3).

The synthesis of **27** suggested that this concept was correct. The phenyl ring of **27** conferred a 10-fold potency improvement relative to the methyl substituent. This provided the impetus to begin a full scale effort to optimize the amide in conjunction with the pyrrolopyrimidine C-5 substituent³⁷ while maintaining an emphasis on lipophilic efficiency.

We engaged in a focused incorporation of simple substituents expected to maintain clogP < 3. In particular, the ortho and para positions of the benzamide provided efficient locations to introduce substituents; this was most apparent with the fluoro analogues **28**, **29**, and **30**. In all cases, the fluorine substituent provided an increase in potency relative to the unsubstituted phenyl group of **27**. In the ortho-position, this improvement incurred no additional lipophilicity, while in the para-position, the increase in potency was large enough to compensate for the heightened lipophilicity. The higher LipE values for both **28** and **30** reflect the role of the ortho- and para-positions in potency improvement for this series. The small decrease in LipE for **29** versus **27** indicated that the meta-position was potentially less promising for manipulation.

Table 6. SAR of Nonracemic (3*S*)-Amino-aminomethylbenzamide Analogues^a

compd	R	Ph substituent	Akt kinase IC ₅₀ (nM)	Akt cell IC ₅₀ (μ M)	PKA selectivity ratio	LipE	HLM Er	clogP
31	CN	4-F	7.8	5.74	120.3	7	0.26	1.1
32	Me	4-F	3.0	1.46	522	6.5	0.36	2
33	Cl	4-F	2.6	0.36	115.4	6.3	0.55	2.3
34	Et	4-F	1.4	0.65	645	6.3	0.63	2.6
35	CN	4-Cl	17.5	6.34	ND	6.1	0.38	1.6
36	Me	4-Cl	11.4	1.95	51.8	5.3	0.62	2.6
37	Cl	4-Cl	3.3	0.35	39.8	5.6	0.61	2.9
38	Et	4-Cl	1.8	0.92	ND	5.6	0.67	3.1
39	CN	2,4-diF	7.7	1.86	88.4	7.3	0.26	0.9
40	Me	2,4-diF	1.0	0.31	ND	7.2	0.39	1.8
41	Cl	2,4-diF	1.1	0.28	50.9	6.9	0.47	2.1
42	Et	2,4-diF	0.5	0.31	900	6.9	0.56	2.4

^aThe kinase and cell values are reported as the geometric mean of at least two separate determinations, with a typical standard variation of less than $\pm 30\%$.

Once this scan of substituents was complete, sets of compounds were prepared with enantiomerically pure amino-pyrrolidines⁵¹ using multiple pyrrolopyrimidine C-5 core variations (-CN, -Cl, -Me, -Et). Again, a key aspect of the design was to keep the clogP below 3. For a given amide, the trends for potency, selectivity, and in vitro clearance are very consistent (Table 6). Use of a polar core substituent (-CN) at C-5 reduced the log *P* and provided good microsomal stability but attenuated the potency (entries **31**, **35**, and **39**). Compromised potency combined with an apparent permeability issue (in part related to the higher total polar surface area) gave weaker cellular activity for these compounds in an assay measuring the phosphorylation of a known Akt substrate, GSK-3. As the core substituents became more lipophilic (-Me, -Cl, -Et), potency improved and stability was diminished. For benzamide substitution, the 4-Cl analogues (**35**–**38**) all had lower lipophilic efficiency compared with the corresponding 4-F compounds (**31**–**34**), similar to the results observed in the racemic series. Of the substituents examined, the 2,4-difluoro analogues (**39**–**42**) exhibited the best overall potency and metabolic profile.

All of the compounds in Table 6 displayed good selectivity for PKA, and some had extraordinary selectivity. Particularly notable was compound **42**, which achieved 900-fold selectivity for Akt over PKA, presumably because of the increased steric demand of the ethyl core substituent being better tolerated in Akt than in PKA. This, in conjunction with the beneficial effect of the 2,4-difluoro substitution for Akt, provided an extremely selective analogue. After submission of **42** to a panel of 226 kinases, only seven (CDK7, MSK1, MSK2, PKG1 α , RSK2, RSK3, and PKA) showed > 50% inhibition at 1 μ M. After determination of IC₅₀ values, **42** demonstrated > 100-fold selectivity against Akt for all seven kinases.⁵² Cocrystallization of **42** with Akt (Figure 4) showed that the C-3 amine was engaged in the Glu-234 salt bridge, similar to the early analogues. As expected, the 2,4-difluorobenzamide was extended into the accessible pocket in Akt.

On the basis of these in vitro data, a small set of these advanced analogues were put into further studies, including rat and dog pharmacokinetic studies, as well as in vivo models of

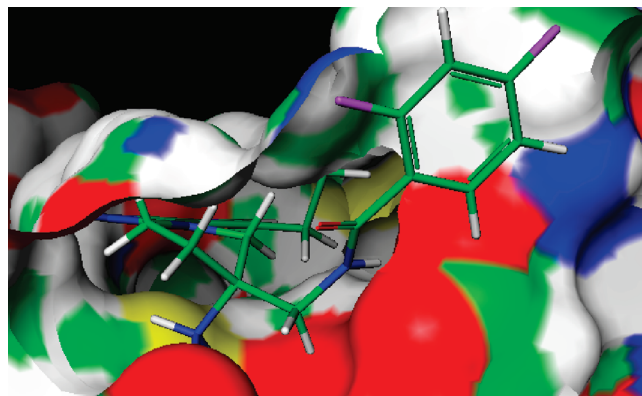


Figure 4. Cocrystal structure of **42** bound to the Akt1 kinase domain.

xenograft tumor progression. On the basis of these data, **42** was chosen as the most promising molecule to advance to clinical development. In vitro, **42** proved highly permeable, and in dog pharmacokinetic studies (oral at 2 mg/kg, iv at 1.2 mg/kg) the compound was well absorbed ($F = 54\%$), with moderate clearance (11.6 (mL/min)/kg) and volume of distribution (4.8 L/kg), and a half-life of 4.4 h. Compound **42** was subsequently evaluated for modulation of Akt in tumors⁵³ and in multiple in vivo mouse models of antitumor efficacy. It was active in a PC3 prostate carcinoma xenograft experiment, with 75% TGI observed at 100 mg/kg b.i.d. dosing for 10 days. In a colorectal carcinoma (Colo205) xenograft study, **42** produced 60% TGI at 150 mg/kg b.i.d. after 10 days. Most intriguingly, in combination with rapamycin (10 mg/kg, ip), 75 mg/kg b.i.d. (10 days) of **42** resulted in 98% TGI in an additional PC3 prostate carcinoma xenograft study compared to 56% TGI and 66% TGI with **42** and rapamycin as single agents. There were no significant toxicological side effects observed in these studies beyond modest weight loss in the highest dosing groups.

Conclusion

In summary, we have outlined the optimization of **2**–**4** to advanced molecules such as **42** using a combination of both

structure- and physical-property-based design parameters. Substituents in place of the C-3 methine proton of the aminopyrrolidine lead **4** served to lock the pseudoaxial disposition of the amine and to provide a platform for optimizing the physical properties of the resulting molecules. Critical in this effort was the understanding of overall lipophilicity and its effect on both potency and in vitro ADME properties. During lead optimization, changes in LipE highlighted valuable structural modifications and discouraged the overuse of lipophilicity, which ultimately provided more balanced molecules. Compound **42** provided significantly enhanced selectivity for Akt relative to earlier leads such as spiroindoline **2**. As a result, **42** was nominated for clinical development and represents a broadly selective, potent, ATP-competitive Akt inhibitor.

Experimental Section

General Experimental Details. All solvents and reagents were obtained from commercially available sources and used without further purification. Reactions were carried out under nitrogen atmosphere unless otherwise described. Flash chromatography purifications were performed on prepacked silica gel cartridges on ISCO CombiFlash Companion systems using the indicated mobile phases. HPLC analysis was performed on an Agilent HP1100 system with an Agilent Zorbax SB-CN column (4.6 mm × 75 mm, 3.5 μm, 1.5 mL/min flow rate), mobile phase (H₂O/0.1% HClO₄)/(ACN/0.1% HClO₄) (90:10 at 0 min to 10:90 at 5 min). All tested compounds prepared as solids were determined to be >95% pure at 210 nm. LC/MS STD refers to a Polaris C18A column (2.0 mm × 20 mm, 5 μm, 1.0 mL/min flow rate); mobile phase A of 94.95% H₂O, 5% CAN, 0.05% formic acid; mobile phase B of 99.95% CAN, 0.05% formic acid; A/B ratios of 95:5 at 0 min, 80:20 at 1 min, 50:50 at 2.3 min, and 0:100 at 3.6 min, with compound detection by UV and MS. LC/MS Polar refers to a Polaris C18A column (2.0 mm × 20 mm, 5 μm, 1.0 mL/min flow rate), mobile phase A of 94.95% H₂O, 5% ACN, 0.05% formic acid; mobile phase B of 99.95% ACN, 0.05% Fformic acid; A/B ratios of 95:5 at 0 min, 80:20 at 2 min, 50:50 at 2.3 min, and 0:100 at 3.6 min, with compound detection by UV and MS. Mass spectral data were collected on a Micromass ADM atmospheric pressure chemical ionization instrument (LRMS APCI). NMR spectra were generated on a Varian 400 MHz or a Varian 500 MHz instrument as indicated. Chemical shifts were recorded in ppm relative to tetramethylsilane (TMS) with multiplicities given as s (singlet), bs (broad singlet), d (doublet), t (triplet), dt (double of triplets), m (multiplet).

Assay Description. Akt1 Kinase Assay. A fluorescence polarization IMAP type assay is used. An amount of 15 μL of diluted test compound in DMSO is mixed with 60 μL of reaction buffer (10 mM Tris-HCl, pH 7.5, 10 mM MgCl₂, 0.1 mM EGTA, 0.01% Triton-X100, 1 mM DTT). Then 5 μL of the compound/buffer mixture, 10 μL of a solution containing 4 μM ATP and 40 nM fluorescent-labeled Crosstide (Tamara-labeled GRPR-TSSFAEG peptide), and 5 μL of Akt1 protein (lacking the pleckstrin homology (PH) domain, containing an Asp at position 473, and prephosphorylated at Thr 308) in reaction buffer are combined. After a 90 min incubation, IMAP beads are added and plates are read (lamp filter, 544 nm; emission filter, 615 nm). The same procedure can be applied to full length Akt1 to provide similar results. All IC₅₀ values are the geometric mean of at least *n* = 2 determinations.

PKA Kinase Assay. A fluorescence polarization IMAP (Molecular Devices Corp.) type assay is used. An amount of 15 μL of diluted test compound in DMSO is mixed with 60 μL of reaction buffer (10 mM Tris-HCl, pH 7.5, 10 mM MgCl₂, 0.1 mM EGTA, 0.01% Triton-X100, 1 mM DTT). Then 5 μL of the compound/buffer mixture, 10 μL of a solution containing 4 μM ATP and 40 nM fluorescent-labeled Kempptide (Tamara-labeled LRRASLG

peptide), and 5 μL of recombinant PKA catalytic subunit (Upstate Biotechnology, catalog number 14-440) in reaction buffer are combined. After a 90 min incubation, IMAP beads are added and plates are read (lamp filter, 544 nm; emission filter, 615 nm). All IC₅₀ values are the geometric mean of at least *n* = 2 determinations.

Akt Cell Assay. The phosphorylation status of an Akt substrate, GSK-3α, in the U87 glioblastoma line was measured as an indicator of cellular activity. U87 cells (10 000) were plated overnight in DMEM medium containing 15% fetal calf serum (FCS) and incubated with compound (seven concentrations plus vehicle) for 2 h in DMEM medium lacking FCS. After cell lysis, 45% of the lysate was transferred to a 96-well, flat bottom, black polystyrene plate (Costar, catalog number 3295) previously coated in a stepwise fashion with 100 μL/well of goat antirabbit IgG (Pierce Corp., catalog number 31210) diluted to 5 μg/mL in carbonate–bicarbonate buffer (Sigma, catalog number C-3041), followed by TBST washing (Sigma, catalog number T-9039), blocking in 5% BSA/TBST, and addition of 100 μL/well of a phosphospecific antibody to GSK-3α/β (Cell Signaling Technology, catalog number 9331) used at 0.06 μg/mL. After subsequent washing and blocking steps, cell lysate was added and incubated for 1 h at ambient temperature with shaking. The plates were then washed four times with TBST. To detect bound phospho-GSK-3α, 70 μL of a 1:1000 dilution of anti-GSK-3α was added (Santa Cruz, catalog number SC-5264). Plates were incubated for 1 h at ambient temperature with shaking, and washed four times with TBST. After washing, 70 μL/well of a 1:5000 dilution of goat antimouse-HRP (Jackson Labs, catalog number 115-035-146) in 5% BSA/TBST was added. Plates were incubated for 1 h at ambient temperature with shaking, washed, and 70 μL/well of SuperSignal ELISA PICO Maximum Sensitivity Substrate (Pierce Corp., catalog number 37075) was added. Signal was allowed to develop for 1 min, and plates were read on a Victor luminometer. The signal obtained from wells containing lysis buffer only (no cell control) was subtracted before IC₅₀ values were calculated. All IC₅₀ values are the geometric mean of at least *n* = 2 determinations.

1-(5-Methyl-7H-pyrrolo[2,3-d]pyrimidin-4-yl)-3-(phenylamino)methylpyrrolidin-3-amine (19). A mixture of aniline (0.16 mL, 1.77 mmol) and 3 Å molecular sieves (0.5 g) was added to a solution of *tert*-butyl 3-formyl-1-(5-methyl-7H-pyrrolo[2,3-d]pyrimidin-4-yl)pyrrolidin-3-ylcarbamate **17** (0.5 g, 1.45 mmol), glacial acetic acid (1 mL), and MeOH (9 mL). The resulting reaction mixture was stirred at 25 °C overnight, treated with MP-cyanoborohydride (1.45 g, 2.5 mmol/g, 3.65 mmol), and stirred for an additional 5 h. The mixture was filtered, and the solids were rinsed with MeOH. The combined organic phases were concentrated to provide *tert*-butyl 1-(5-methyl-7H-pyrrolo[2,3-d]pyrimidin-4-yl)-3-((phenylamino)methyl)pyrrolidin-3-ylcarbamate, which was treated directly with DCM (10 mL) and TFA (10 mL), and the resultant reaction mixture was stirred at 25 °C for 3 h. The mixture was concentrated, and the residue was purified by chromatography on silica gel (eluting with dichloromethane, with a gradient ramp to 1% aqueous NH₄OH, 29% MeOH, 70% DCM) to provide 1-(5-methyl-7H-pyrrolo[2,3-d]pyrimidin-4-yl)-3-((phenylamino)methyl)pyrrolidin-3-amine (**19**). Yield: 325 mg, 1.01 mmol, 70%. APCI MS+ (*M* + 1) = 323.2. ¹H NMR (500 MHz, methanol-*d*₄) δ ppm 2.03 (1H, m), 2.21 (1H, m), 2.38 (3H, s), 3.37 (2H, m), 3.68 (1H, d), 3.89 (1H, d), 3.91 (1H, m), 4.05 (1H, q), 6.60 (1H, t), 6.69 (2H, d), 6.92 (1H, s), 7.08 (2H, m), 8.08 (1H, s).

N-((3-Amino-1-(5-methyl-7H-pyrrolo[2,3-d]pyrimidin-4-yl)pyrrolidin-3-yl)methyl)benzamide (27). A solution of 3-(aminomethyl)-*N*-(2,4-dimethoxybenzyl)-1-(5-methyl-7H-pyrrolo[2,3-d]pyrimidin-4-yl)pyrrolidin-3-amine (50 mg, 0.13 mmol) in DMF (1.2 mL) was treated with 1-hydroxybenzotriazole (HOBT) (26 mg, 0.19 mmol), benzoic acid (16 mg, 0.13 mmol), and PS-carbodiimide (160 mg, 0.25 mmol). The resultant reaction mixture was stirred at 25 °C for 6 h, treated with MP-carbonate (160 mg,

0.5 mmol), and stirred overnight. The mixture was filtered, and the solids were rinsed with MeOH. The combined filtrates were evaporated, and the residue was treated with TFA (0.5 mL) and heated at 80 °C for 3 h. The reaction mixture was concentrated, and the residue was purified by preparative RP-HPLC (TFA/ACN/H₂O) to provide *N*-((3-amino-1-(5-methyl-7*H*-pyrrolo[2,3-*d*]pyrimidin-4-yl)pyrrolidin-3-yl)methyl)benzamide (**27**). Yield: 12 mg, 26% for two steps. MS⁺ (M + 1)⁺: 351.3. *t*_R (LCMS standard): 0.7 min. ¹H NMR (400 MHz, methanol-*d*₄) δ ppm 8.03 (s, 1 H), 7.82 (d, *J* = 7.48 Hz, 2 H), 7.53 (t, *J* = 7.06 Hz, 1 H), 7.40–7.49 (m, 2 H), 6.90 (s, 1 H), 3.85–4.05 (m, 3 H), 3.54–3.68 (m, 3 H), 3.31 (s, 2 H), 2.39 (s, 3 H), 2.08–2.19 (m, 1 H), 1.92–2.01 (m, 1 H).

N-((3-Amino-1-(5-methyl-7*H*-pyrrolo[2,3-*d*]pyrimidin-4-yl)pyrrolidin-3-yl)methyl)-4-fluorobenzamide (**30**). Compound **30** was prepared by an identical sequence of reactions as was used to prepare **27** but using 4-fluorobenzoic acid in place of benzoic acid. ¹H NMR (DMSO-*d*₆) δ ppm 11.3 (bs, 1H), 8.56 (t, *J* = 5.7 Hz, 1H), 8.04 (s, 1H), 7.94 (dd, *J* = 8.8, 5.7 Hz, 2H), 7.30 (dd, *J* = 8.8, 8.8 Hz, 2H), 6.93 (s, 1H), 3.88–3.82 (m, 1H), 3.75–3.71 (m, 1H), 3.68 (d, *J* = 10.9 Hz, 1H), 3.47 (m, 3H), 2.31 (s, 3H), 1.95–1.73 (m, 4H).

(*S*)-*N*-((3-Amino-1-(5-ethyl-7*H*-pyrrolo[2,3-*d*]pyrimidin-4-yl)pyrrolidin-3-yl)methyl)-2,4-difluorobenzamide (**42**). A mixture of (*R*)-*N*-((3-aminopyrrolidin-3-yl)methyl)-2,4-difluorobenzamide (16 g, 49 mmol), 4-chloro-5-ethyl-7*H*-pyrrolo[2,3-*d*]pyrimidine (8.9 g, 49 mmol), and sodium bicarbonate (20.5 g, 244 mmol) in ethanol (150 mL) was refluxed for 10 h. The mixture was then filtered hot through Celite, and the filtrate was concentrated under reduced pressure. The resultant residue was partitioned between EtOAc (100 mL) and water (200 mL), and the organic phase was collected. The aqueous phase was extracted with ethyl acetate (2 × 100 mL), and the combined organic extracts were washed with water (2 × 100 mL), brine (80 mL), dried over Na₂SO₄, filtered, and concentrated under reduced pressure to provide (*S*)-*N*-((3-amino-1-(5-ethyl-7*H*-pyrrolo[2,3-*d*]pyrimidin-4-yl)pyrrolidin-3-yl)methyl)-2,4-difluorobenzamide (**42**) as a pale-yellow solid. Yield: 17.4 g, 89.3%. TLC *R*_f = 0.42 (10% methanol/CH₂Cl₂). APCI MS⁺ (M + 1) = 402.1. ¹H NMR (500 MHz, methanol-*d*₄) δ ppm 8.07 (s, 1 H), 7.80 (q, *J* = 8.64 Hz, 1 H), 7.10 (q, *J* = 8.12 Hz, 2 H), 6.94 (s, 1 H), 3.98 (m, 3 H), 3.65 (m, 3 H), 2.87 (q, *J* = 7.08 Hz, 2 H), 2.17 (m, 1 H), 1.97 (m, 1 H), 1.30 (t, *J* = 7.26 Hz, 3 H).

Acknowledgment. The authors want to thank Katherine Brightly for extremely helpful advice in manuscript preparation and editing.

Supporting Information Available: Experimental details for key intermediates and for compounds **31–41**; details of the X-ray crystallography and pharmacokinetic and pharmacodynamic studies. This material is available free of charge via the Internet at <http://pubs.acs.org>.

References

- Bellacosa, A.; Testa, J. R.; Staal, S. P.; Tschlis, P. N. A retroviral oncogene, akt, encoding a serine–threonine kinase containing an SH2-like region. *Science* **1991**, *254*, 274–277.
- Altomare, D. A.; Testa, J. R. Perturbations of the AKT signaling pathway in human cancer. *Oncogene* **2005**, *24*, 7455–7464.
- Dudek, H.; Datta, S. R.; Franke, T. F.; Birnbaum, M. J.; Yao, R.; Cooper, G. M.; Segal, R. A.; Kaplan, D. R.; Greenberg, M. E. Regulation of neuronal survival by the serine–threonine protein kinase Akt. *Science* **1997**, *275*, 661–665.
- Nicholson, K. M.; Anderson, N. G. The protein kinase B/Akt signalling pathway in human malignancy. *Cell. Signalling* **2002**, *14*, 381–395.
- Cheng, J. Q.; Lindsley, C. W.; Cheng, G. Z.; Yang, H.; Nicosia, S. V. The Akt/PKB pathway: molecular target for cancer drug discovery. *Oncogene* **2005**, *24*, 7482–7492.
- Vlietstra, R. J.; Van Alewijk, D. C. J. G.; Hermans, K. G. L.; Van Steenbrugge, G. J.; Trapman, J. Frequent inactivation of PTEN in prostate cancer cell lines and xenografts. *Cancer Res.* **1998**, *58*, 2720–2723.
- Yuan, Z. Q.; Sun, M.; Feldman, R. I.; Wang, G.; Ma, X.-L.; Jiang, C.; Coppola, D.; Nicosia, S. V.; Cheng, J. Q. Frequent activation of AKT2 and induction of apoptosis by inhibition of phosphoinositide-3-OH kinase/Akt pathway in human ovarian cancer. *Oncogene* **2000**, *19*, 2324–2330.
- Tokunaga, E.; Kimura, Y.; Oki, E.; Ueda, N.; Futatsugi, M.; Mashino, K.; Yamamoto, M.; Ikebe, M.; Kakeji, Y.; Baba, H.; Maehara, Y. Akt is frequently activated in HER2/neu-positive breast cancers and associated with poor prognosis among hormone-treated patients. *Int. J. Cancer* **2005**, *118*, 284–289.
- Tokunaga, E.; Kataoka, A.; Kimura, Y.; Oki, E.; Mashino, K.; Nishida, K.; Koga, T.; Morita, M.; Kakeji, Y.; Baba, H.; Ohno, S.; Maehara, Y. The association between Akt activation and resistance to hormone therapy in metastatic breast cancer. *Eur. J. Cancer* **2006**, *42*, 629–635.
- Hennessy, B. T.; Smith, D. L.; Ram, P. T.; Lu, Y.; Mills, G. B. Exploiting the PI3K/AKT pathway for cancer drug discovery. *Nat. Rev. Drug Discovery* **2005**, *4*, 988–1004.
- Yap, T. A.; Garrett, M. D.; Walton, M. I.; Raynaud, F.; de Bono, J. S.; Workman, P. Targeting the PI3K–AKT–mTOR pathway: progress, pitfalls, and promises. *Curr. Opin. Pharmacol.* **2008**, *8*, 393–412.
- Garcia-Echeverria, C.; Sellers, W. R. Drug discovery approaches targeting the PI3K/Akt pathway in cancer. *Oncogene* **2008**, *27*, 5511–5526.
- Lindsley, C. W.; Barnett, S. F.; Layton, M. E.; Bilodeau, M. T. The PI3K/Akt pathway: recent progress in the development of ATP-competitive and allosteric Akt kinase inhibitors. *Curr. Cancer Drug Targets* **2008**, *8*, 7–18.
- Cheng, G. Z.; Park, S.; Shu, S.; He, L.; Kong, W.; Zhang, W.; Yuan, Z.; Wang, L.-H.; Cheng, J. Q. Advances of AKT pathway in human oncogenesis and as a target for anti-cancer drug discovery. *Curr. Cancer Drug Targets* **2008**, *8*, 2–6.
- Meric-Bernstam, F.; Gonzalez-Angulo, A. M. Targeting the mTOR signaling network for cancer therapy. *J. Clin. Oncol.* **2009**, *27*, 2278–2287.
- Ayral-Kaloustian, S.; Gu, J.; Lucas, J.; Cinque, M.; Gaydos, C.; Zask, A.; Chaudhary, I.; Wang, J.; Di, L.; Young, M.; Ruppen, M.; Mansour, T. S.; Gibbons, J. J.; Yu, K. Hybrid inhibitors of phosphatidylinositol 3-kinase (PI3K) and the mammalian target of rapamycin (mTOR): design, synthesis, and superior antitumor activity of novel wortmannin–rapamycin conjugates. *J. Med. Chem.* **2010**, *53*, 452–459.
- Sun, C. L.; Li, X. Rapamycin Analogs as Anti-Cancer Agents. *WO/2009/131631*, 2009.
- Chresta, C. M.; Davies, B. R.; Hickson, I.; Harding, T.; Cosulich, S.; Critchlow, S. E.; Vincent, J. P.; Ellston, R.; Jones, D.; Sini, P.; James, D.; Howard, Z.; Dudley, P.; Hughes, G.; Smith, L.; Maguire, S.; Hummersone, M.; Malagu, K.; Menear, K.; Jenkins, R.; Jacobsen, M.; Smith, G. C. M.; Guichard, S.; Pass, M. AZD8055 is a potent, selective, and orally bioavailable ATP-competitive mammalian target of rapamycin kinase inhibitor with in vitro and in vivo antitumor activity. *Cancer Res.* **2010**, *70*, 288–298.
- Marone, R.; Cmiljanovic, V.; Giese, B.; Wymann, M. P. Targeting phosphoinositide 3-kinase—moving towards therapy. *Biochim. Biophys. Acta, Proteins Proteomics* **2008**, *1784*, 159–185.
- Folkes, A. J.; Ahmadi, K.; Alderton, W. K.; Alix, S.; Baker, S. J.; Box, G.; Chuckowree, I. S.; Clarke, P. A.; Depledge, P.; Eccles, S. A.; Friedman, L. S.; Hayes, A.; Hancox, T. C.; Kugendradas, A.; Lensun, L.; Moore, P.; Olivero, A. G.; Pang, J.; Patel, S.; Pergl-Wilson, G. H.; Raynaud, F. I.; Robson, A.; Saghir, N.; Salphati, L.; Sohal, S.; Ultsch, M. H.; Valenti, M.; Wallweber, H. J. A.; Wan, N. C.; Wiesmann, C.; Workman, P.; Zhyvoloup, A.; Zvelebil, M. J.; Shuttleworth, S. J. The identification of 2-(1*H*-indazol-4-yl)-6-(4-methanesulfonyl-piperazin-1-ylmethyl)-4-morpholin-4-yl-thieno[3,2-*d*]pyrimidine (GDC-0941) as a potent, selective, orally bioavailable inhibitor of class I PI3 kinase for the treatment of cancer. *J. Med. Chem.* **2008**, *51*, 5522–5532.
- Lohar, M. V.; Mundada, R.; Bhonde, M.; Padgaonkar, A.; Deore, V.; Yewalkar, N.; Bhatia, D.; Rathos, M.; Joshi, K.; Vishwakarma, R. A.; Kumar, S. Design and synthesis of novel furoquinoline based inhibitors of multiple targets in the PI3K/Akt-mTOR pathway. *Bioorg. Med. Chem. Lett.* **2008**, *18*, 3603–3606.
- Fan, Q.-W.; Knight, Z. A.; Goldenberg, D. D.; Yu, W.; Mostov, K. E.; Stokoe, D.; Shokat, K. M.; Weiss, W. A. A dual PI3 kinase/mTOR inhibitor reveals emergent efficacy in glioma. *Cancer Cell* **2006**, *9*, 341–349.
- Maira, S.-M.; Stauffer, F.; Brueggen, J.; Furet, P.; Schnell, C.; Fritsch, C.; Brachmann, S.; Chene, P.; De Pover, A.; Schoemaker, K.; Fabbro, D.; Gabriel, D.; Simonen, M.; Murphy, L.; Finan, P.;

- Sellers, W.; Garcia-Echeverria, C. Identification and characterization of NVP-BEZ235, a new orally available dual phosphatidylinositol 3-kinase/mammalian target of rapamycin inhibitor with potent in vivo antitumor activity. *Mol. Cancer Ther.* **2008**, *7*, 1851–1863.
- (24) Saxty, G.; Woodhead, S. J.; Berdini, V.; Davies, T. G.; Verdonk, M. L.; Wyatt, P. G.; Boyle, R. G.; Barford, D.; Downham, R.; Garrett, M. D.; Carr, R. A. Identification of inhibitors of protein kinase B using fragment-based lead discovery. *J. Med. Chem.* **2007**, *50*, 2293–2296.
- (25) Lin, X.; Murray, J. M.; Rico, A. C.; Wang, M. X.; Chu, D. T.; Zhou, Y.; Del Rosario, M.; Kaufman, S.; Ma, S.; Fang, E.; Crawford, K.; Jefferson, A. B. Discovery of 2-pyrimidyl-5-amidothiophenes as potent inhibitors for AKT: synthesis and SAR studies. *Bioorg. Med. Chem. Lett.* **2006**, *16*, 4163–4168.
- (26) Woods, K. W.; Fischer, J. P.; Claiborne, A.; Li, T.; Thomas, S. A.; Zhu, G.-D.; Diebold, R. B.; Liu, X.; Shi, Y.; Klinghofer, V.; Han, E. K.; Guan, R.; Magnone, S. R.; Johnson, E. F.; Bouska, J. J.; Olson, A. M.; de Jong, R.; Oltersdorf, T.; Luo, Y.; Rosenberg, S. H.; Giranda, V. L.; Li, Q. Synthesis and SAR of indazole-pyridine based protein kinase B/Akt inhibitors. *Bioorg. Med. Chem.* **2006**, *14*, 6832–6846.
- (27) Donald, A.; McHardy, T.; Rowlands, M. G.; Hunter, L.-J. K.; Davies, T. G.; Berdini, V.; Boyle, R. G.; Aherne, G. W.; Garrett, M. D.; Collins, I. Rapid evolution of 6-phenylpurine inhibitors of protein kinase B through structure-based design. *J. Med. Chem.* **2007**, *50*, 2289–2292.
- (28) Zhu, G.-D.; Gong, J.; Gandhi, V. B.; Woods, K.; Luo, Y.; Liu, X.; Guan, R.; Klinghofer, V.; Johnson, E. F.; Stoll, V. S.; Mamo, M.; Li, Q.; Rosenberg, S. H.; Giranda, V. L. Design and synthesis of pyridine-pyrazolopyridine-based inhibitors of protein kinase B/Akt. *Bioorg. Med. Chem.* **2007**, *15*, 2441–2452.
- (29) Zhu, G.-D.; Gandhi, V. B.; Gong, J.; Thomas, S.; Woods, K. W.; Song, X.; Li, T.; Diebold, R. B.; Luo, Y.; Liu, X.; Guan, R.; Klinghofer, V.; Johnson, E. F.; Bouska, J.; Olson, A.; Marsh, K. C.; Stoll, V. S.; Mamo, M.; Polakowski, J.; Campbell, T. J.; Martin, R. L.; Gintant, G. A.; Penning, T. D.; Li, Q.; Rosenberg, S. H.; Giranda, V. L. Syntheses of potent, selective, and orally bioavailable indazole-pyridine series of protein kinase B/Akt inhibitors with reduced hypotension. *J. Med. Chem.* **2007**, *50*, 2990–3003.
- (30) Caldwell, J. J.; Davies, T. G.; Donald, A.; McHardy, T.; Rowlands, M. G.; Aherne, G. W.; Hunter, L. K.; Taylor, K.; Ruddle, R.; Raynaud, F. I.; Verdonk, M. D.; Workman, P.; Garrett, M. D.; Collins, I. Identification of 4-(4-aminopiperidin-1-yl)-7H-pyrrolo[2,3-d]pyrimidines as selective inhibitors of protein kinase B through fragment elaboration. *J. Med. Chem.* **2008**, *51*, 2147–2157.
- (31) Zhao, Z.; Robinson, R. G.; Barnett, S. F.; Defeo-Jones, D.; Jones, R. E.; Hartman, G. D.; Huber, H. E.; Duggan, M. E.; Lindsley, C. W. Development of potent, allosteric dual Akt1 and Akt2 inhibitors with improved physical properties and cell activity. *Bioorg. Med. Chem. Lett.* **2008**, *18*, 49–53.
- (32) Lindsley, C. W.; Zhao, Z.; Leister, W. H.; Robinson, R. G.; Barnett, S. F.; Defeo-Jones, D.; Jones, R. E.; Hartman, G. D.; Huff, J. R.; Huber, H. E.; Duggan, M. E. Allosteric Akt (PKB) inhibitors: discovery and SAR of isozyme selective inhibitors. *Bioorg. Med. Chem. Lett.* **2005**, *15*, 761–764.
- (33) Zhao, Z.; Leister, W. H.; Robinson, R. G.; Barnett, S. F.; Defeo-Jones, D.; Jones, R. E.; Hartman, G. D.; Huff, J. R.; Huber, H. E.; Duggan, M. E.; Lindsley, C. W. Discovery of 2,3,5-trisubstituted pyridine derivatives as potent Akt1 and Akt2 dual inhibitors. *Bioorg. Med. Chem. Lett.* **2005**, *15*, 905–909.
- (34) Siu, T.; Li, Y.; Nagasawa, J.; Liang, J.; Tehrani, L.; Chua, P.; Jones, R. E.; Defeo-Jones, D.; Barnett, S. F.; Robinson, R. G. The design and synthesis of potent and cell-active allosteric dual Akt 1 and 2 inhibitors devoid of hERG activity. *Bioorg. Med. Chem. Lett.* **2008**, *18*, 4191–4194.
- (35) Siu, T.; Liang, J.; Arruda, J.; Li, Y.; Jones, R. E.; Defeo-Jones, D.; Barnett, S. F.; Robinson, R. G. Discovery of potent and cell-active allosteric dual Akt 1 and 2 inhibitors. *Bioorg. Med. Chem. Lett.* **2008**, *18*, 4186–4190.
- (36) Wu, Z.; Robinson, R. G.; Fu, S.; Barnett, S. F.; Defeo-Jones, D.; Jones, R. E.; Kral, A. M.; Huber, H. E.; Kohl, N. E.; Hartman, G. D.; Bilodeau, M. T. Rapid assembly of diverse and potent allosteric Akt inhibitors. *Bioorg. Med. Chem. Lett.* **2008**, *18*, 2211–2214.
- (37) Bilodeau, M. T.; Balitz, A. E.; Hoffman, J. M.; Manley, P. J.; Barnett, S. F.; Defeo-Jones, D.; Haskell, K.; Jones, R. E.; Leander, K.; Robinson, R. G.; Smith, A. M.; Huber, H. E.; Hartman, G. D. Allosteric inhibitors of Akt1 and Akt2: a naphthyridinone with efficacy in an A2780 tumor xenograft model. *Bioorg. Med. Chem. Lett.* **2008**, *18*, 3178–3182.
- (38) Li, Y.; Liang, J.; Siu, T.; Hu, E.; Rossi, M. A.; Barnett, S. F.; Defeo-Jones, D.; Jones, R. E.; Robinson, R. G.; Leander, K.; Huber, H. E.; Mittal, S.; Cosford, N.; Prasit, P. Allosteric inhibitors of Akt1 and Akt2: discovery of [1,2,4]triazolo[3,4-f][1,6]naphthyridines with potent and balanced activity. *Bioorg. Med. Chem. Lett.* **2009**, *19*, 834–836.
- (39) Lippa, B.; Pan, G.; Corbett, M.; Li, C.; Kauffman, G. S.; Pandit, J.; Robinson, S.; Wei, L.; Kozina, E.; Marr, E. S.; Borzillo, G.; Knauth, E.; Barbacci-Tobin, E. G.; Vincent, P.; Troutman, M.; Baker, D.; Rajamohan, F.; Kakar, S.; Clark, T.; Morris, J. Synthesis and structure based optimization of novel Akt inhibitors. *Bioorg. Med. Chem. Lett.* **2008**, *18*, 3359–3363.
- (40) Heering, D. A.; Rhodes, N.; Leber, J. D.; Clark, T. J.; Keenan, R. M.; Lafrance, L. V.; Li, M.; Safonov, I. G.; Takata, D. T.; Venslavsky, J. W.; Yamashita, D. S.; Choudhry, A. E.; Copeland, R. A.; Lai, Z.; Schaber, M. D.; Tummino, P. J.; Strum, S. L.; Wood, E. R.; Duckett, D. R.; Eberwein, D.; Knick, V. B.; Lansing, T. J.; McConnell, R. T.; Zhang, S. Y.; Minthorn, E. A.; Concha, N. O.; Warren, G. L.; Kumar, R. Identification of 4-(2-(4-amino-1,2,5-oxadiazol-3-yl)-1-ethyl-7-((3S)-3-piperidinylmethyl)oxy)-1H-imidazo[4,5-c]pyridin-4-yl)-2-methyl-3-butyn-2-ol (GSK690693), a novel inhibitor of AKT kinase. *J. Med. Chem.* **2008**, *51*, 5663–5679.
- (41) Unpublished results.
- (42) Tomita, K.; Tsuzuki, Y.; Shibamori, K.-i.; Tashima, M.; Kajikawa, F.; Sato, Y.; Kashimoto, S.; Chiba, K.; Hino, K. Synthesis and structure-activity relationships of novel 7-substituted 1,4-dihydro-4-oxo-1-(2-thiazolyl)-1,8-naphthyridine-3-carboxylic acids as antitumor agents. Part 1. *J. Med. Chem.* **2002**, *45*, 5564–5575.
- (43) Much of the SAR was developed in the racemic series, with periodic checks to confirm that the trend of improved potency and selectivity was consistently achieved with a single enantiomer. This was true in all cases examined, and the absolute stereochemistry was determined for advanced analogues (cf. Table 6).
- (44) Obach, R. S. The prediction of human clearance from hepatic microsomal metabolism data. *Curr. Opin. Drug Discovery Dev.* **2001**, *4*, 36–44.
- (45) Diaz, G. J.; Daniell, K.; Leitza, S. T.; Martin, R. L.; Su, Z.; McDermott, J. S.; Cox, B. F.; Gintant, G. A. The [³H]dofetilide binding assay is a predictive screening tool for hERG blockade and proarrhythmia: comparison of intact cell and membrane preparations and effects of altering [K⁺]_o. *J. Pharmacol. Toxicol. Methods* **2004**, *50*, 187–199.
- (46) Finlayson, K.; Sharkey, J. A High-Throughput Binding Assay for hERG. In *Optimization in Drug Discovery: In Vitro Methods*; Yan, Z., Caldwell, G. W., Eds.; Methods in Pharmacology and Toxicology; Springer: Secaucus, NJ; 2004; pp 353–368.
- (47) Finlayson, K.; Turnbull, L.; January, C. T.; Sharkey, J.; Kelly, J. S. [³H]Dofetilide binding to hERG transfected membranes: a potential high throughput preclinical screen. *Eur. J. Pharmacol.* **2001**, *430*, 147–148.
- (48) Leeson, P. D.; Springthorpe, B. The influence of drug-like concepts on decision-making in medicinal chemistry. *Nat. Rev. Drug Discovery* **2007**, *6*, 881–890.
- (49) Ryckmans, T.; Edwards, M. P.; Horne, V. A.; Correia, A. M.; Owen, D. R.; Thompson, L. R.; Tran, I.; Tutt, M. F.; Young, T. Rapid assessment of a novel series of selective CB2 agonists using parallel synthesis protocols: a lipophilic efficiency (LipE) analysis. *Bioorg. Med. Chem. Lett.* **2009**, *19*, 4406–4409.
- (50) Mai, K.; Patil, G. Asymmetric synthesis of α -aminonitriles. *Synth. Commun.* **1984**, *14*, 1299–1304.
- (51) Corbett, M. S.; Kauffman, G. S.; Freeman-Cook, K. D.; Lippa, B. S.; Luzzio, M. J.; Morris, J. Amine Derivatives Useful as Anticancer Agents and Their Preparation, Pharmaceutical Compositions and Use in the Treatment of Neoplasm. 2007-1B20652008012635, 20070713, 2008.
- (52) Like all analogues tested, **42** remained relatively unselective among Akt isoforms with IC₅₀ values of 9 and 12 nM against Akt2 and Akt3, respectively.
- (53) See Supporting Information sections VI and VII for a full description of rat and dog pharmacokinetic studies, protein binding data, and mouse pharmacodynamic models measuring mouse exposure and phospho-Akt induction in tumors.